

Supplement of Biogeosciences, 16, 3491–3506, 2019
<https://doi.org/10.5194/bg-16-3491-2019-supplement>
© Author(s) 2019. This work is distributed under
the Creative Commons Attribution 4.0 License.



Supplement of

Assessing the peatland hummock–hollow classification framework using high-resolution elevation models: implications for appropriate complexity ecosystem modeling

Paul A. Moore et al.

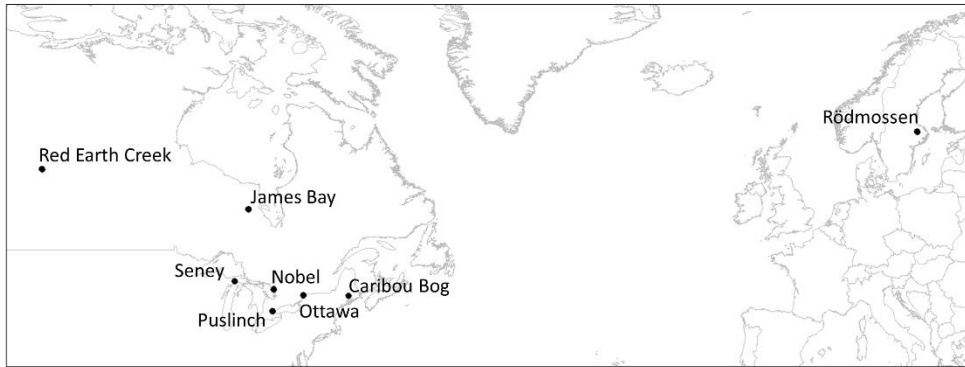
Correspondence to: Paul A. Moore (paul.moore82@gmail.com)

The copyright of individual parts of the supplement might differ from the CC BY 4.0 License.

[Figure S1]

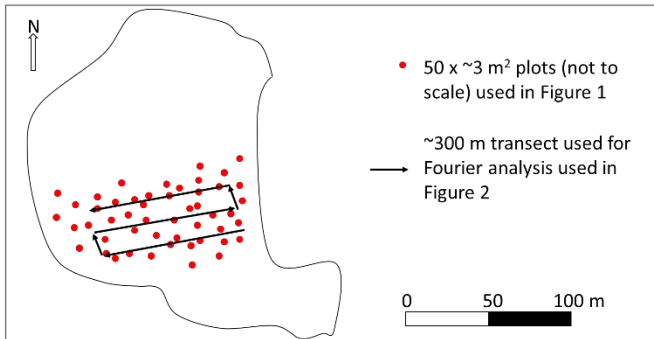
Overview of site locations and measurement design.

Site locations



Red Earth Creek – site-level analysis

- Outline of Red Earth Creek site, plot and transect locations
- Plot locations chosen independent of microtopography
- Same transect design used at Nobel site for site-level analysis.



Plot-level analysis of hummock-hollow pairs:

- Overhead view example of digital elevation model (DEM) for Seney – WET
- SfM-derived DEMs for qualitative and random plots form the basis for analysis presented in Figures 3–10 and all supplemental figures with the exception of Figure S5

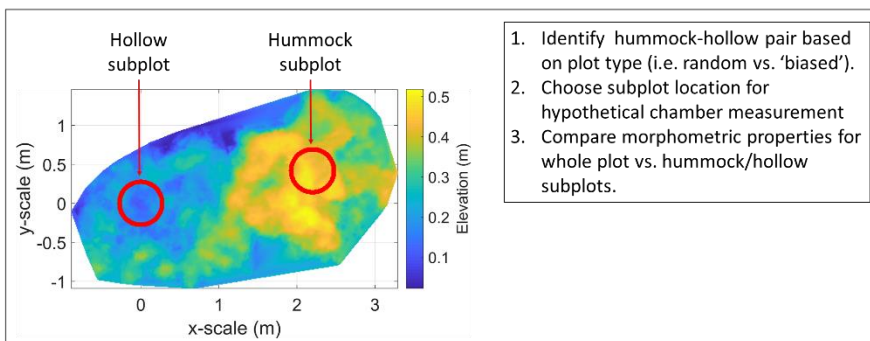


[Figure S2]

Spatial validation of structure-from-motion (SfM) method for lab (a-c) and field (d-f) microtopography. SfM reconstructions, manual measurements, and differences between the two are shown in the top (a, d), middle (b, e), and bottom panels (c, f), respectively.

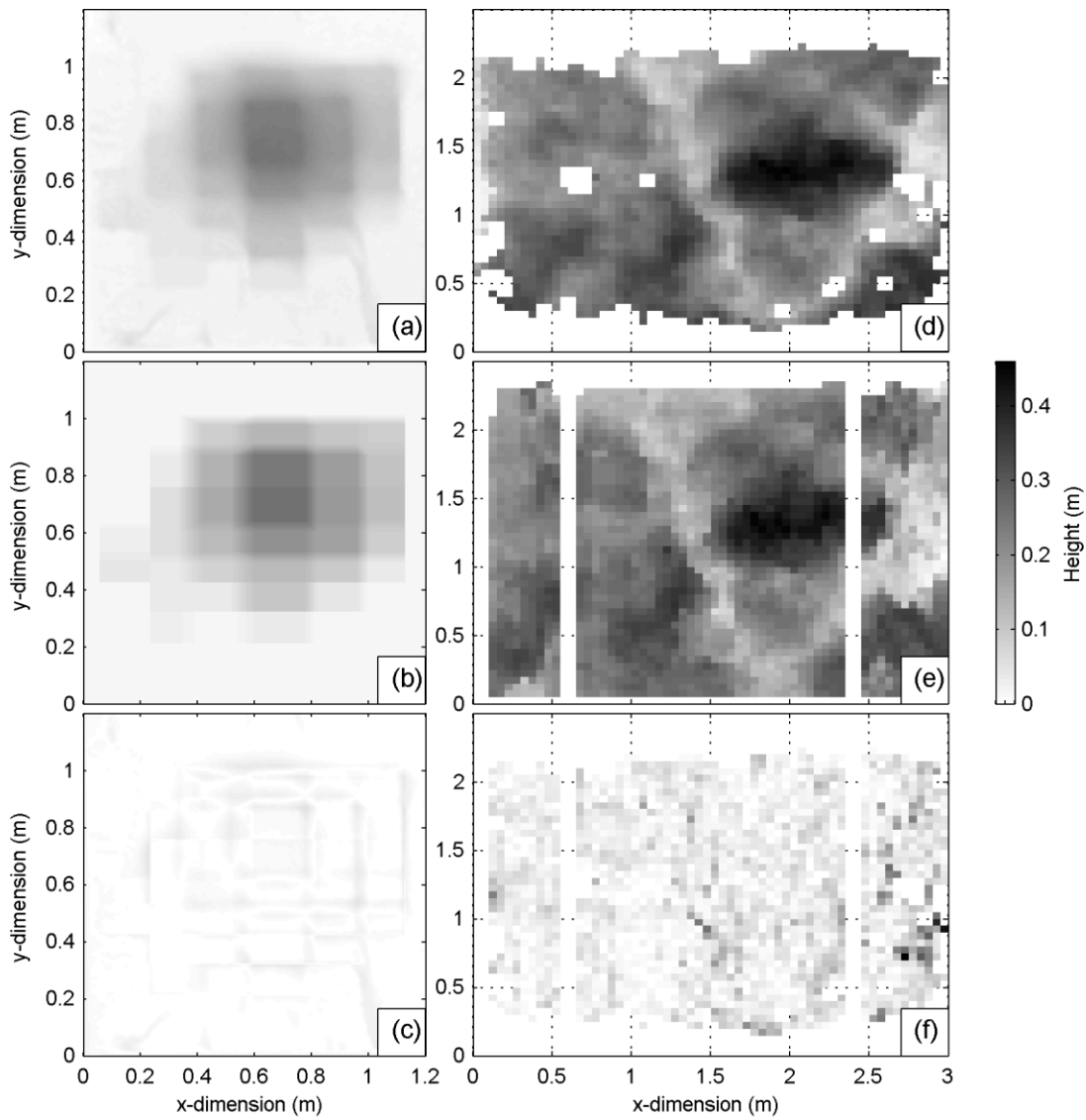


[Figure S3]

Distribution of residuals between structure-from-motion reconstruction and manual elevation measurements (a). Relation between magnitude of residuals and local slope (b). Results are bin averaged, where each point is based on 150, and 1000 measurements for the field and lab tests, respectively. Error bars indicate the standard error. There is a degree of pseudo-replication in lab-based elevation measurements, where flat objects on a flat, level surface were used to construct the synthetic hummock. So, within a particular x-y domain, a single elevation measurement was replicated at the resolution of the DEM.

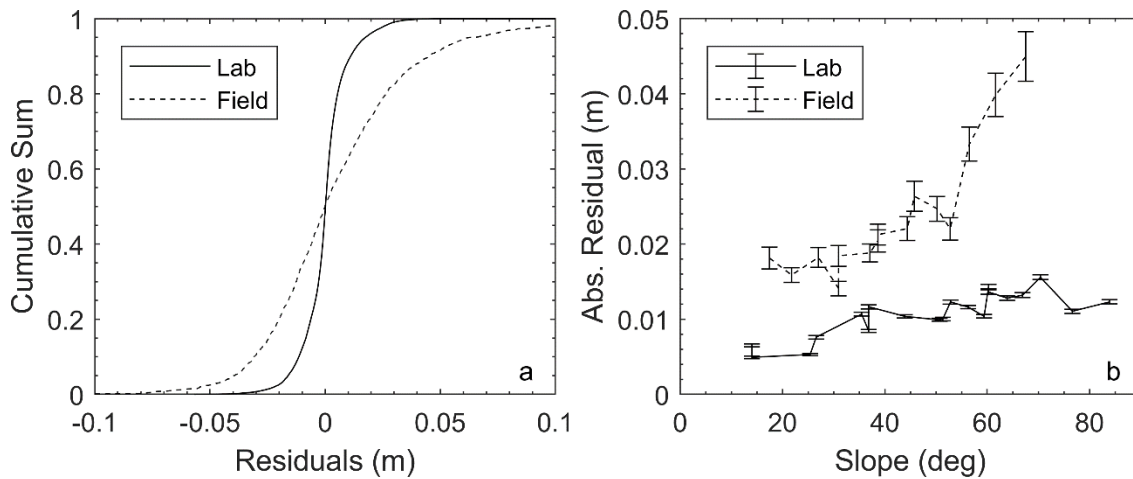


[Figure S4]

Example of unsupervised classification of microtopographic elevation for the Seney, MI WET site (top panel) using *k*-means clustering (middle panel). Black, grey, and white classifications correspond with high-, intermediate-, and low elevation classifications. Microtopography was classified using three clusters based on a post hoc analysis of elevation distributions by Gaussian mixture models. The lower panel shows the distribution of height in the high- (solid), intermediate- (dot-dashed), and low- (dashed) elevation classifications. We term these microtopographic classes as high hummock, low hummock, and hollow/lawn.

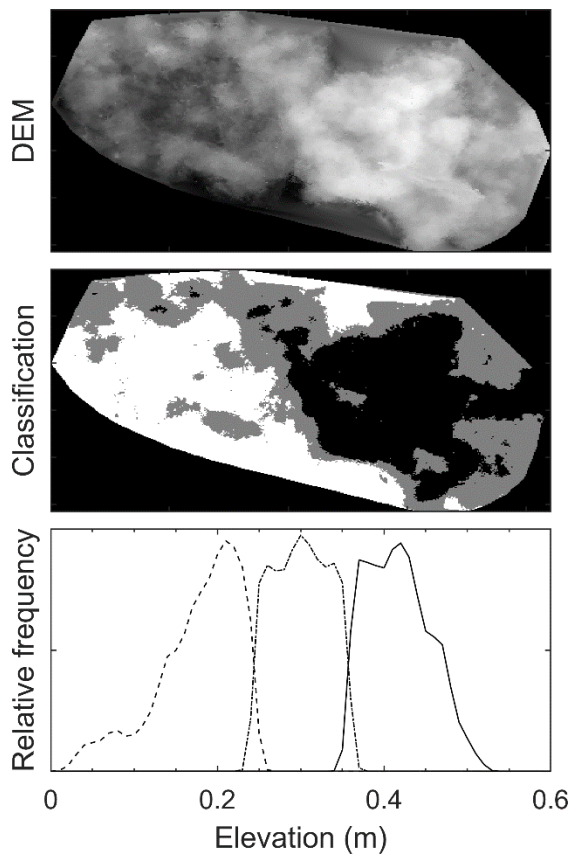
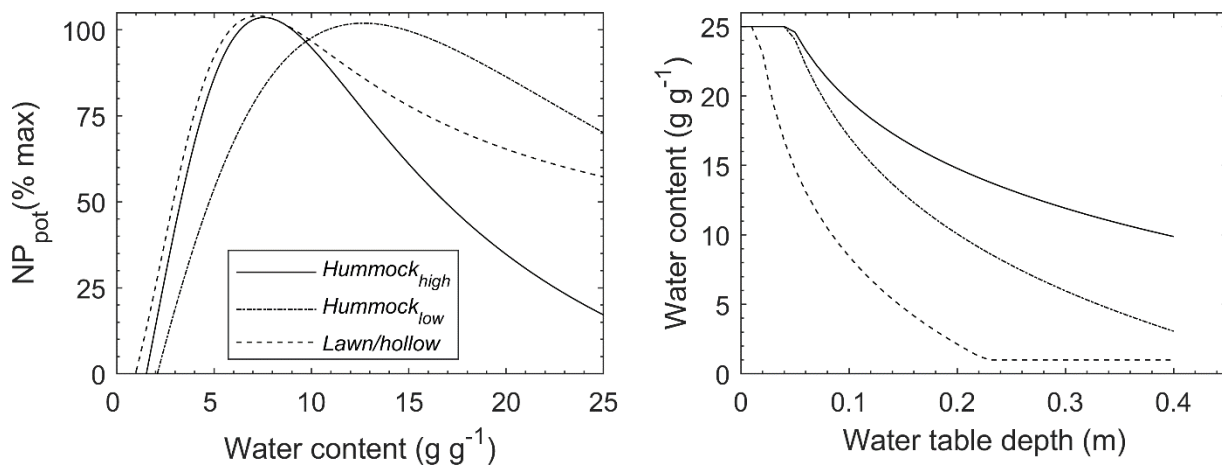


[Figure S5]

Empirical relations for normalized moss capitula potential net photosynthesis (NP_{pot} - % of maximum) (a), and moss water content ($g_{water} g^{-1}_{dry\ weight}$) (b). Empirical relations were parameterized for high hummocks, low hummocks, and lawn/hollows using *Sphagnum* species of the section Acutifolia, *Sphagnum*, and *Cuspidata*, respectively. NP_{pot} was parameterized using data for *Sphagnum fuscum*¹, *S. papillosum*¹, and *S. cuspidatum*¹, respectively. Water content was parameterized using data for *Sphagnum fuscum*², *S. magellanicum*², and *S. tenellum*³, respectively.



¹ – Schipperges, B., and Rydin, H.: Response of photosynthesis of *Sphagnum* species from contrasting microhabitats to tissue water content and repeated desiccation, *New Phytologist*, 140(4), 677-684, 1998.

² – Strack, M., and Price, J.S.: Moisture controls on carbon dioxide dynamics of peat - *Sphagnum* monoliths. *Ecohydrology*, 2(1), 34-41, doi: 10.1002/eco.36, 2009

³ – Rydin, H.: Effect of water level on desiccation of *Sphagnum* in relation to surrounding Sphagna, *Oikos*, 45(3), 374-379, doi: 10.2307/3565573, 1985.

[Figure S6]

Combined relative frequency distribution of all plots (n=9) at the NOBEL, ON site (Table 1) compared to the combined distribution of all Nobel, ON hummock-hollow subplots. Whole plot locations at the NOBEL, ON site where chosen randomly, with a perceived hummock-hollow microform identified around the random point. For each subplot, a location for a hummock and hollow subplot was identified in order to compare morphometric properties at spatial scales typical of chamber flux measurement compared to the microform as a whole.

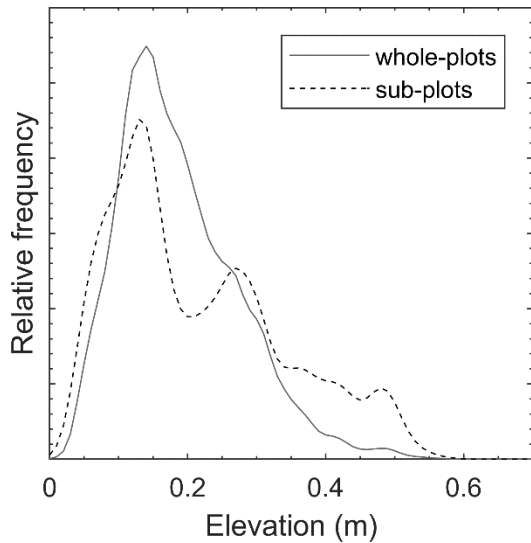


[Figure S7]

Gaussian mixture model (GMM) fit to relative frequency distribution of measured microtopographic elevation for four example plots. The full GMM distribution is obtained by summing the individual members. Examples for two- (upper panels) and three- member (lower panels) GMMs are given for elevation distributions which qualitatively show a separation of modes (left panels) versus ones where modes are not visually distinct (right panels).

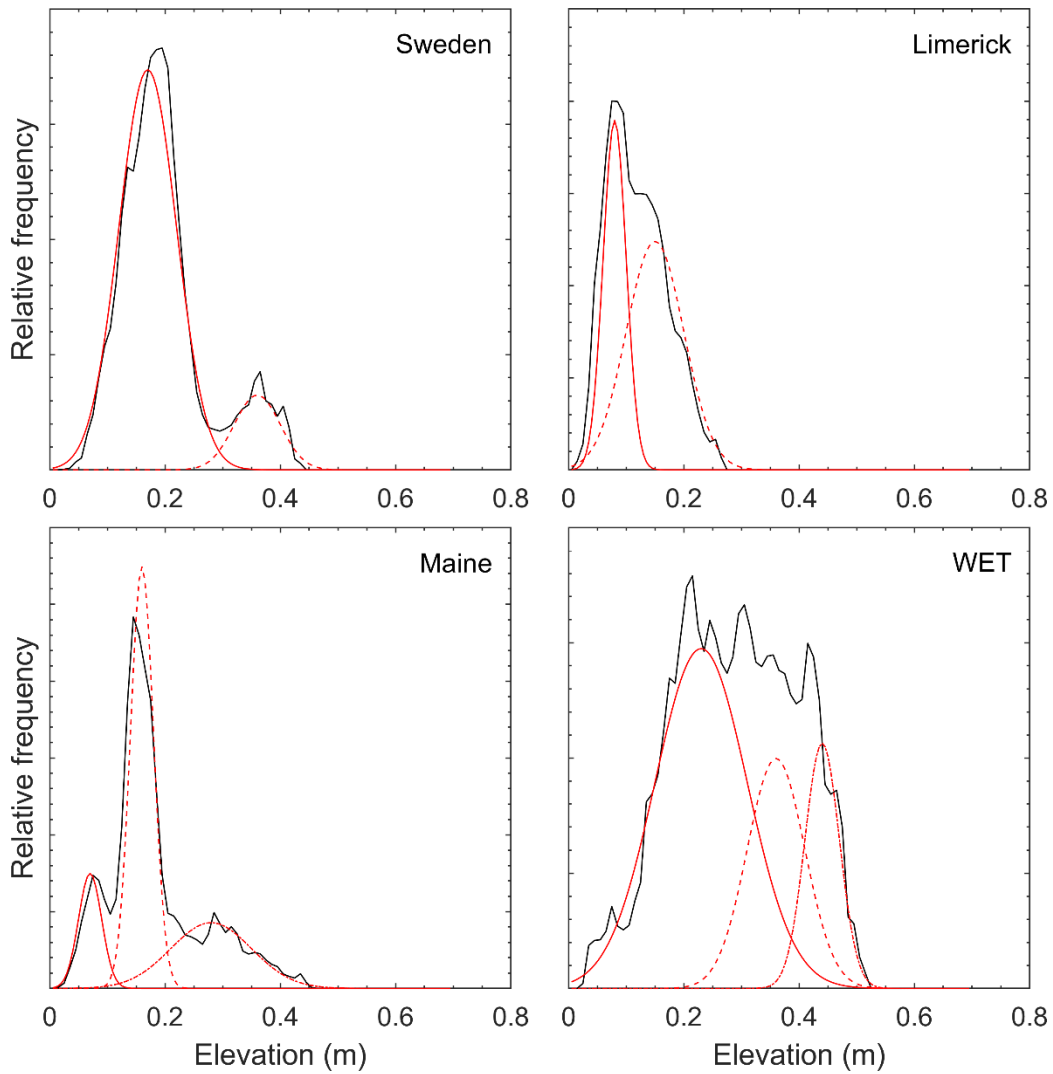


[Figure S8]

Frequency distribution showing goodness of fit of measured and modelled slope for two sample microtopography plots at NOBEL, ON site. Slope is derived from the surface normal of planar fit to elevation in a moving 0.03 m x 0.03 m window for the Alpha and Zeta DEM plots. A Weibull probability distribution is used to model slope distribution at the scale of interest. A Weibull distribution was chosen over other candidate models (i.e. Gamma, log-logistic, and log-normal) based on goodness of fit (AIC) across all plots (n=18).

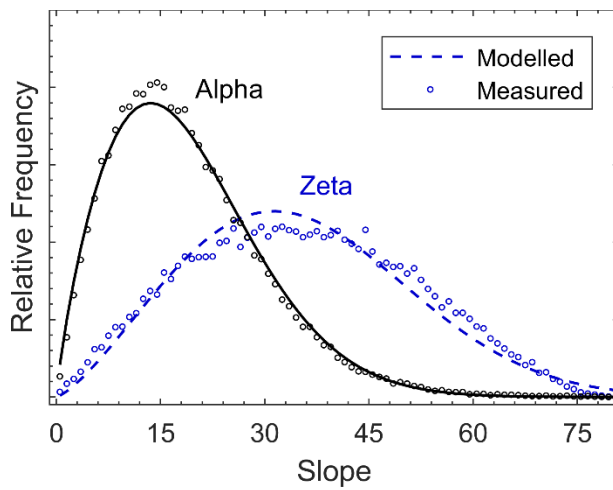


[Figure S9]

Comparison of modal slope from Weibull distribution fit (left panel) and frequency of steep slope (i.e. $>45^\circ$) (right panel). Boxplots show median (circle with dot), interquartile range (black box), and outliers (open circles) for hummock and hollow subplots as well as high-, intermediate-, and low-elevation GMM clusters.

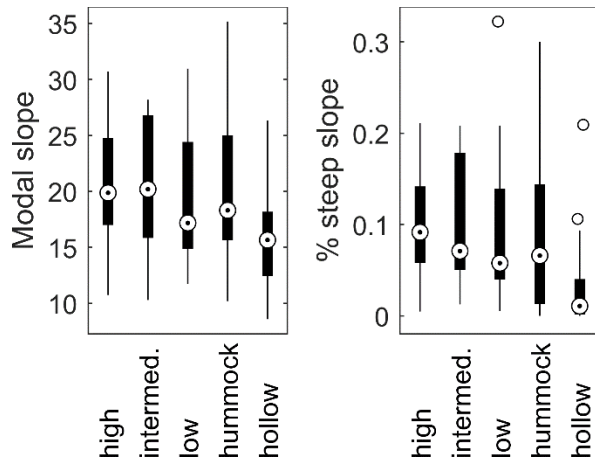


[Figure S10]

Variation in potential solar insolation relative to a flat surface based on aspect for randomly (a) and qualitatively chosen plots (b). Median of aspect-binned values are plotted.

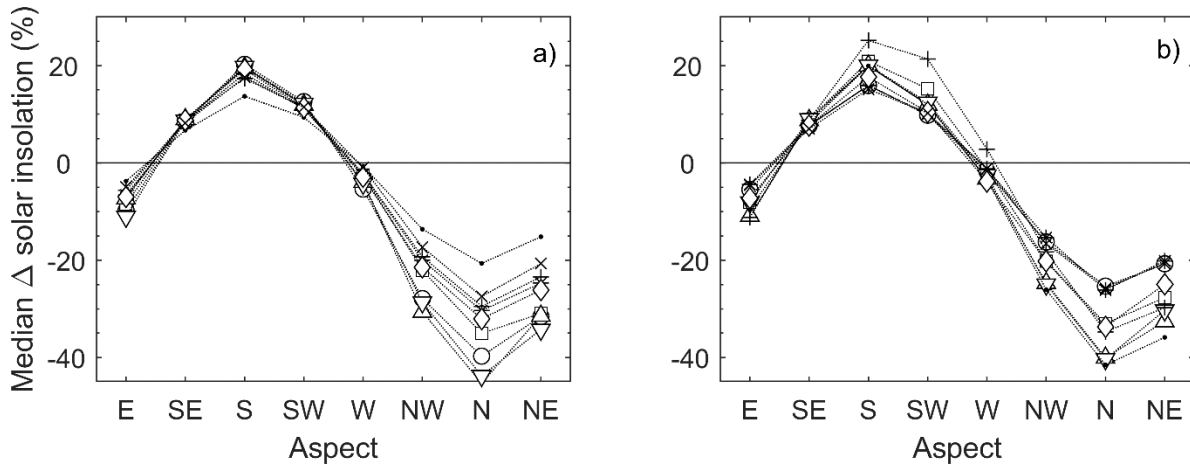


[Figure S11]

Potential net photosynthesis (NP_{pot}) for three microtopographic classes (e.g. see Figure S4) for random (a) and qualitatively chosen (b) plots. NP_{pot} -WC and WC-WTD relations are based on a common parameterization (see Figure S5 — low hummock). Although the whole plot is modelled using the low hummock parameterization, areas previously classified as high/low hummock and lawn/hollow are labelled as such for comparison to model with independent parameterization for each class (see Figure 8).

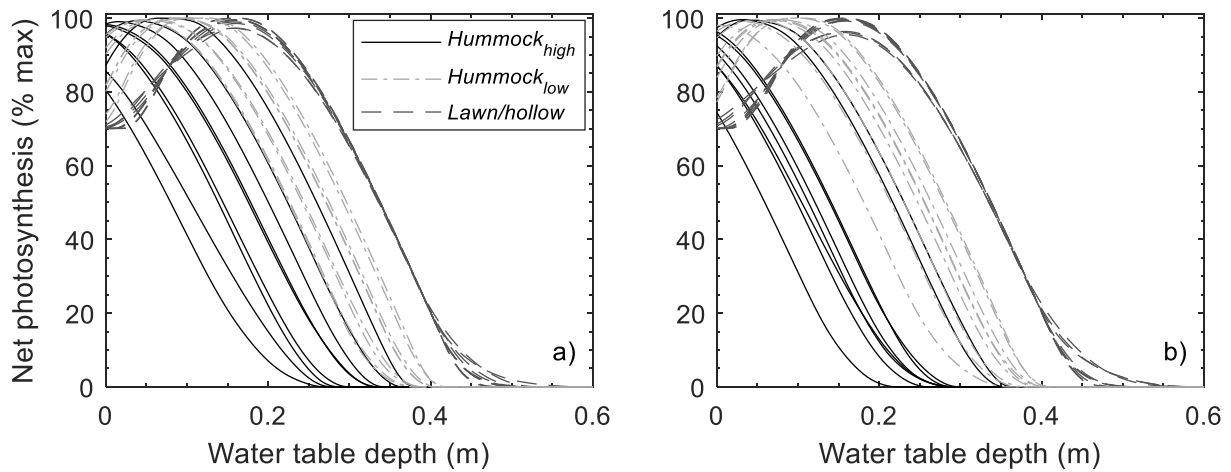


[Figure S12]

Modelled potential net photosynthesis (NP_{pot}) based on uniform parameterization (bottom row) and parameterization based on microtopographic class (middle row). Empirical relations are shown in Figure S5, where the low-hummock relations are used for the uniform parameterization. Examples are modelled for three water table depths (WTD) relative to the average hollow/lawn elevation. Microtopographic parameterization is based on unsupervised k-means classification of elevation (upper left panel) with plot area classified as hollow/lawn (blue), low-hummock (black) and high-hummock (red) (upper middle panel).

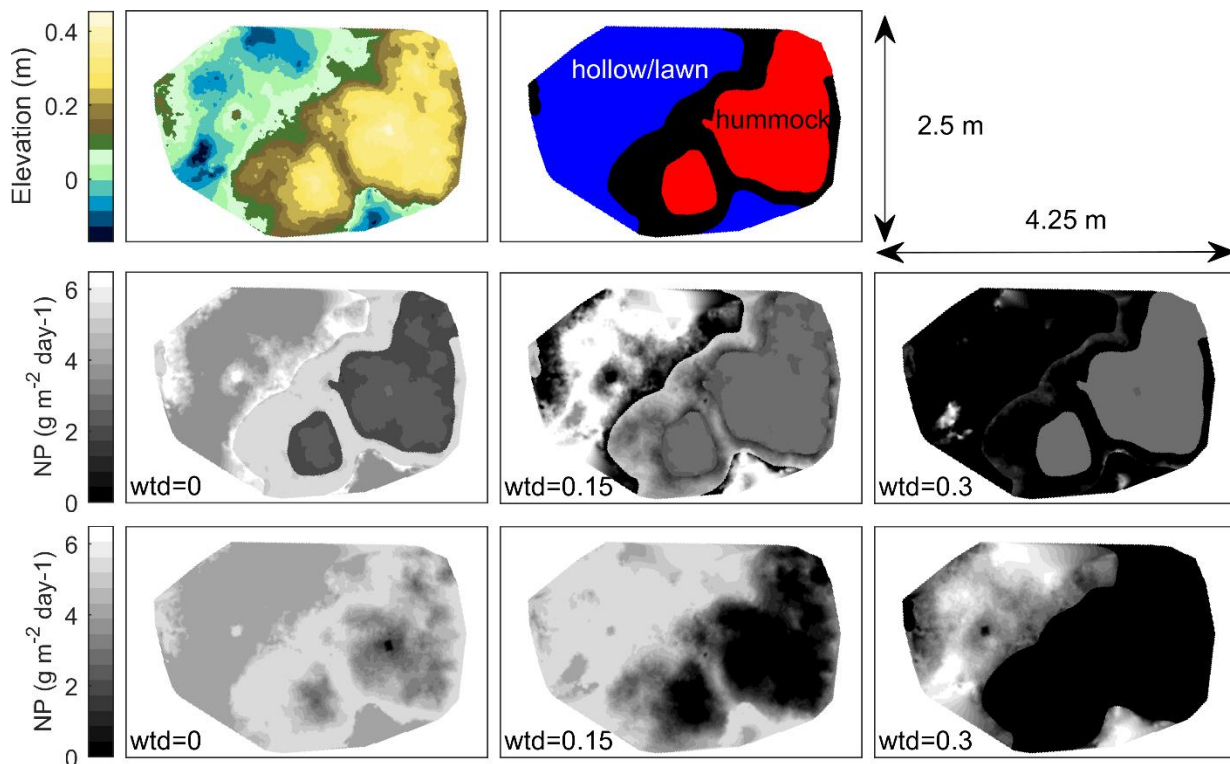


[Figure S13]

Example spatial distribution of elevation for the Seney-INT plot where the DEM has been discretized using the specified number of elevation values (n_z), where 'full' corresponds with the original DEM. Discretized elevation values are based on elevation percentiles ($p_{z,i}$) where $p_{z,i} = (i - 1) \frac{100}{n_z} + \frac{50}{n_z}$; for $i=1$ to n_z . Elevation is shown relative to lowest point in original DEM plot in metres.

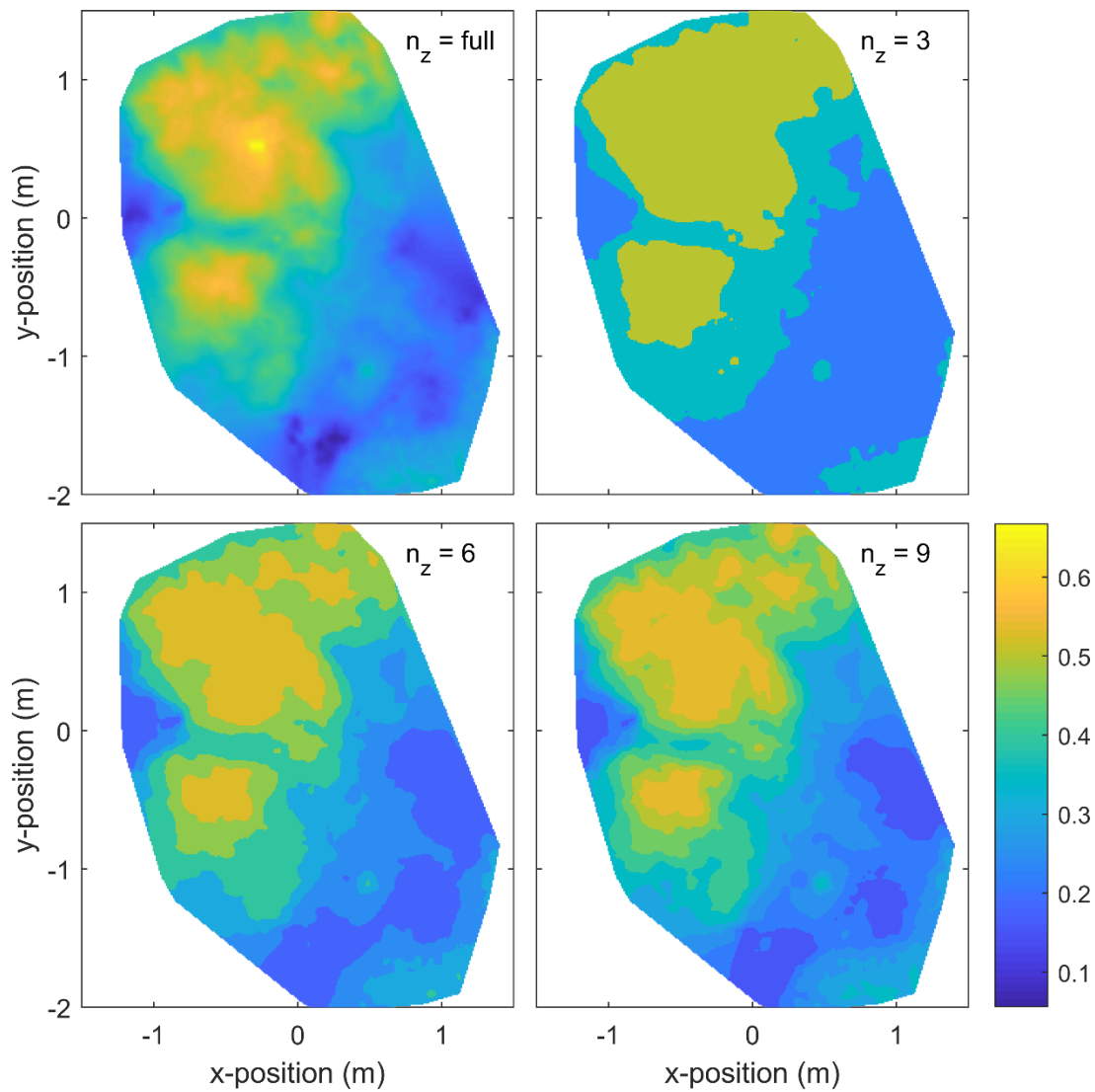


Table S1:

The maximum and root mean square error (RMSE) for the control points in the x-, y-, and z-directions for two laboratory trials.

Axis	Lab trial #1			Lab trial #2		
	RMSE (mm)	Max error (mm)	n	RMSE (mm)	Max error (mm)	n
x	9.5	14	9	3.3	12	49
y	2.9	5	9	2.9	7	47
z	3.1	6	9	4.3	9	46

Section S1: Validation measurements

While the structure-from-motion (SfM) approach is well validated (e.g. *Fonstad et al., 2013; Nouwakpo et al., 2014*), we sought to characterize the potential resolution and accuracy of our implementation of the method in peatlands. We carried out two lab-based trials, as well as manual measurements of microtopography for a target area in the field. The first lab trial tested the potential accuracy of the SfM method as implemented in this study. Using nine reference objects of known dimension (29 mm × 29 mm × 29 mm and 29 mm × 29 mm × 60 mm) and position (9 × 9 grid, 317 mm spacing) on a flat, square, 1267 mm × 1267 mm surface, a point cloud was generated for the target area. The square surface was used as a reference object for scaling the SfM-derived point cloud. The second lab trial involved constructing a synthetic hummock from wood blocks to produce a complex shape of known position and geometry. The synthetic hummock was draped with a mottled green sheet to emulate a moss surface, while also masking sharp edges that could enhance feature detection. Finally, we took detailed manual measurements of microtopographic variation for one of our plots (Puslinch site; see Table 1 main text) for comparison to the DEM derived from the SfM method. For manual measurements of the Puslinch plot, a rigid frame was mounted and levelled above the plot. The surface height was then measured to the nearest 0.01 m on a 0.05 m × 0.05 m grid pattern.

Laboratory trials of the SfM method demonstrated reasonable accuracy for reconstructing the target objects. For the first lab trial, the point cloud reconstruction had an average RMSE of 0.005 m and a maximum error of 0.014 m (Table S1) in comparison to the known size and position of the reference blocks. The more detailed spatial comparison for both

the second lab and field validation measurements showed that the shape, size, and orientation of microforms are reproducible to a reasonable degree of accuracy. For example, the field-based reconstruction (Figure S2d-f) clearly shows two major features of the measured microtopography (Figure S2e), namely: the oval-shaped hummock on the centre-right; and the small gully running vertically through the middle of the plot. Residuals from the lab measurements (Figure S2c) are systematically linked to either transition points between blocks, or unmeasured irregularities on the sheet covering the target surface. In the case of field measurements (Figure S2f), the spatial arrangement of comparatively high residual values appears more random. The median absolute deviation for the lab (trial #2) and field measurements are 0.004 m ($n=1.0 \times 10^5$) and 0.018 m ($n=2.9 \times 10^3$), respectively (Figure S3a). Figure S3b shows that relatively large residuals for both field and lab measurements correlate with areas of rapid change in surface elevation. A portion of the error may be the result of small inaccuracies in the manual survey rather than solely from the SfM method itself. For example, where the local slope is 60° , positional errors in the x-y direction from the manual survey can introduce error in the z-measurement by up to 1.7 times the x-y error (*i.e.*, $\cos(30^\circ)/\cos(60^\circ)$).

References:

Fonstad, M. A., Dietrich, J. T., Courville, Jensen, J. L., and Carbonneau, P. E.: Topographic structure from motion: a new development in photogrammetric measurement, *Earth Surface Processes and Landforms*, 38(4), 421-430, doi: 10.1002/esp.3366, 2013.

Nouwakpo, S. K., James, M. R., Weltz, M. A., Huang, C. H., Chagas, I., and Lima, L.: Evaluation of structure from motion for soil microtopography measurement, *The Photogrammetric Record*, 29(147), 297-316, doi: 10.1111/phor.12072, 2014.